ISSN 2079-1704. Хімія, фізика та технологія поверхні. 2024. Т. 15. № 3. С. 328-339

PACS 33.50.-j doi: 10.15407/hftp15.03.328

O.Yu. Semchuk, O.O. Havryliuk, A.A. Biliuk

INDUCTIVE-RESONANCE ENERGY TRANSFER IN HYBRID CARBON NANOSTRUCTURES

Chuiko Institute of Surface Chemistry of National Academy of Sciences of Ukraine
17 General Naumov Str., Kyiv, 03164, Ukraine, E-mail: aleksandr1950@meta.ua

Based on the first principles, we have shown that the decisive role in energy transfer from the fluorophore molecule to the carbon substrate (graphene) is played by the Förster-type inductive-resonance energy transfer mechanism. The Förster energy transfer rate can be calculated analytically via Fermi's golden rule with the momentum-dependent initial final states of the graphene substrates and the HOMO (the highest occupied molecular orbital) and LUMO (the lowest unoccupied molecular orbital) states of the dye molecule. Combining first-principle calculations characterizing the hybrid carbon nanomaterials with tight-binding-based consideration of graphene wave functions allows us to obtain an analytical expression for the Förster energy transfer rate. We constructed graphical dependences of the Förster energy transfer rate at the distance R between substrate (graphene) and dye molecule for several materials. The results obtained can be applied to various hybrids based on carbon nanostructures and in general to the description of energy transfer processes in molecular functionalized nanostructures, once the molecular dipole moment and the substrate - molecule separation are known.

Keywords*: graphene, carbon nanotubes, functionalized graphene, dye molecule, Fermi's golden rule, rate of energy transfer, fluorophore molecules, Förster mechanism, Dexter mechanism, optoelectronics*

INTRODUCTION

In recent years there are widely used in optoelectronics many different materials based on hybridized carbon in its low dimensional forms, such as carbon nanotubes, graphene quantum dots, graphene nanoribbons and functionalized graphene. Such materials are already widely used in highly efficient photovoltaic devices and for biomedical imaging and sensing. In this regard, there is an increased interest in hybrid materials consisting of graphene functionalized with due molecules. The first experiments on similar systems were recently implemented, which illustrates the extremely efficient transfer of excitation energy from an adsorbed molecule to a carbon substrate (graphene). Until now, there was no microscopically justified explanation of how energy is transferred in such systems. In connection with the aggravation of the problem of stability and duration of operation of optoelectronic devices based on organic materials, the task of finding new approaches to the creation of materials that could eliminate these shortcomings has arisen. In this connection, the search for new materials and new functional elements becomes relevant. This explains the interest in new hybrid nanosystems based on hybridized carbon in its low dimensional forms, such as carbon nanotubes, graphene quantum dots, graphene nanoribbons and functionalized graphene. They consist of small-sized nanostructures functionalized with the help of a separate molecule, which combines the excellent properties of both subsystems. Therefore, carbon nanostructures are excellent substrates, after which they show high sensitivity to changes in their environment [1–7]. The first experiments were conducted that illustrate the successful functionality of carbon nanotubes with photoactive molecules [8, 9]. Recently, strong excitation and energy transfer have been observed in perylene- and porphyrin-functionalized carbon nanotubes [10–12]. The first studies of functionalized graphene structures also demonstrate high rates of energy transfer between attached molecules and the graphene layer [13]. The combination of unique transport properties of graphene, including ballistic transport and strong absorption of light by organic molecules, leads to the emergence of new hybrid nanostructures with great application potential for highly efficient photodetectors, biomedical sensors, and photovoltaic devices [8, 9]. The observed energy transfer can be explained on the basis of two mechanisms of nonradiative energy transfer: inductive-resonant (Förster type) [14] and exchange-resonant (also

called Dexter) [15] energy transfer mechanisms. Förster's mechanism describes the direct non-radiative energy transfer from the optically excited dye molecule to the carbon substrate. The rate of energy transfer in such a mechanism strongly depends on the dipole moment of the molecular transition and shows a dependence R^{-4} (at distances R greater than 10 nm) for hybrid nanostructures, in contrast to the well-known scaling dependence for Förster dipolar coupling in molecule-molecule complexes (where distance dependence of order R^{-6}). The Dexter mechanism is based on the transfer of a charge (electron) from an excited dye molecule (donor) to a carbon substrate (acceptor) graphene [15]. As a result, the carbon substrate becomes excited and can emit light through carrier recombination. This mechanism is effective at short distances and depends on the spatial overlap of the orbital functions of the dye molecule and graphene, which leads to its exponential decay with the substrate–molecule distance.

In this paper, we reviewed the main existing theoretical approaches used to describe energy transfer in carbon-based hybrid nanomaterials, such as carbon nanotubes, graphene quantum dots, graphene nanoribbons, and functionalized graphene. The combination of first-order calculations characterizing hybrid carbon nanomaterials with consideration of the wave functions of graphene based on strong coupling allowed us to obtain an analytical expression for the Förster energy transfer rate in such systems. Note that such a comprehensive analysis of the energy transfer process in hybrid carbon nanostructures is being conducted for the first time. In addition, in this paper, using the example of calculating the rate of energy transfer in the dye molecule-graphene system, the limits of the application of long-large behavior of the rate of energy transfer in such systems are outlined for the first time.

THEORETICAL MODEL

This part of this section is devoted to an overview of the main existing theoretical approaches. For the first time, the quantum mechanical theory of non-radiative (resonance) transfer of excitation energy from the donor (excited molecule) to the acceptor (non-excited molecule) was developed quite a long time ago in the papers of Förster [14] and Dexter [15]. For the first time, this theory was applied to calculate the rate of Förster energy transfer from an excited dye molecule to a two-dimensional structure (graphene) in the works of Sebastian K.L. and Swathi R.S. [17–19]. In our paper we will show how these theories can be applied to the study of energy transfer processes in new hybrid nanostructure – graphene functionalized by dye molecule (Fig. 1). Our task is to calculate the rate of energy transfer from the dye molecule to graphene as dependent on the distance between them. There are two main mechanisms of energy transfer from dye molecule to graphene (Fig. 2 *a*): (i) Förster coupling [15] describes a direct nonradiative transfer of energy from the optically excited dye molecule to graphene. (ii) Dexter coupling [16] is based on a charge transfer between the dye molecule and graphene states (Fig. 2 *b*). After the energy transfer processes, the dye molecule is brought into its ground state, and graphene becomes excited and can emit light through carrier (electron) recombination. It is a short-range transfer mechanism that directly depends on the spatial overlap of involved molecule and graphene orbital functions resulting in an exponential decay with the substrate−molecule distance R.

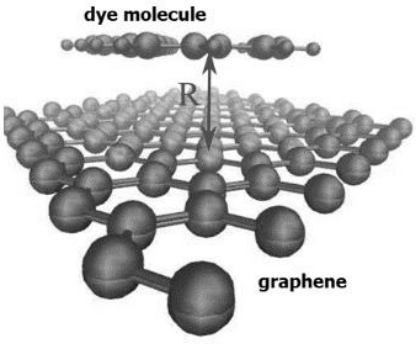

Fig. 1. Schematic representation of functionalized graphene. R – distance between dye molecule and graphene [16]

Förster transfer
a

Dexter transfer
b

Fig. 2. Schematic illustrate of the (*a*) Förster and (*b*) Dexter energy transfer in functionalized graphene. The Dirac cone represent the electronic band structure of graphene, while the electronic states of the dye molecules are described by a two level (HOMO-LUMO) momentum independent system [16]

The Förster (γ_F) and Dexter (γ_D) energy transfer rates can be analytically expressed via the Fermi golden rule [5]:

$$\gamma = \frac{2\pi}{\hbar}\sum_{\vec{k}_i}\sum_{\vec{k}_f}\left|V\left(v\vec{k}_i, c\vec{k}_f, l, h\right)\right|^2 \delta\left(\varepsilon^c_{\vec{k}_f} - \varepsilon^v_{\vec{k}_i} - \Delta E_M\right), \tag{1}$$

$v\vec{k}_i$ – momentum of electrons in the valence band, $c\vec{k}_f$ – momentum of an electron in the conduction band of graphene, ΔE_M – the width of the forbidden zone, $\varepsilon^c_{\vec{k}_f}$ – the energy of an electron in the conduction band of graphene $\varepsilon^v_{\vec{k}_i}$ – energy of an electron in the valence band, with the initial (*i*) and final (*f*) states of the graphene substrate $\Phi^{c/v}_{\vec{k}_i/\vec{k}_f}(\vec{r})$ and the HOMO (*h*) and LUMO (*l*) states in dye molecule $\Phi^{l/h}_M(\vec{r})$. The Förster rate γ_F is determined by the direct contribution of the Coulomb interaction, and the matrix element $V_F\left(v\vec{k}_i, c\vec{k}_f, l, h\right)$ in this case can be written as

$$V_F\left(v\vec{k}_i, c\vec{k}_f, l, h\right) = \\ = \frac{e_0^2}{4\pi\varepsilon_0}\int d\vec{r}\int d\vec{r}'\Phi^{*v}_{\vec{k}_i}(\vec{r})\Phi(\vec{r})^{*c}_{\vec{k}_i}(\vec{r})\left(\frac{1}{|\vec{r}-\vec{r}'|}\right)\Phi^{*l}_M(\vec{r}')\Phi^h_M(\vec{r}'), \tag{2}$$

where e_0 is the electron charge, ε_0 is the dielectric constant.

For the Dexter mechanism (exchange Coulomb contribution) $V_D\left(v\vec{k}_i, c\vec{k}_f, l, h\right)$ can be written as

$$V_D\left(v\vec{k}_i, c\vec{k}_f, l, h\right) = \\ = \frac{e_0^2}{4\pi\varepsilon_0}\int d\vec{r}\int d\vec{r}'\Phi^{*v}_{\vec{k}_i}(\vec{r})\Phi(\vec{r})^h_M(\vec{r})\left(\frac{1}{|\vec{r}-\vec{r}'|}\right)\Phi^{*l}_M(\vec{r}')\Phi^c_{\vec{k}_f}(\vec{r}'). \tag{3}$$

One can see from (1) and (3) that Dexter rate γ_D is determined by the overlap between the strongly localized graphene $\Phi^{*v}_{\vec{k}_i}(\vec{r})$ and dye molecule $\Phi(\vec{r})^h_M(\vec{r})$ orbitals. To estimate the γ_D we must calculate the ratio between the overlaps $\alpha_D = \left\langle \Phi^{*v}_{\vec{k}_i}(\vec{r}) \middle| \Phi(\vec{r})^h_M(\vec{r}) \right\rangle$ and $\alpha_F = \left\langle \Phi^{*v}_{\vec{k}_i}(\vec{r}) \middle| \Phi^c_{\vec{k}_i}(\vec{r}) \right\rangle$ appearing in the Dexter and the Förster rate, respectively. For a number of materials such as porphyrin-functionalized graphene and perylene-functionalized graphene, as was shown in papers [16], $\alpha_D/\alpha_F \approx 10^{-1}$ and because in the rates the square of the product of two such overlaps appears, the Dexter rate γ_D is expected to be approximately 4 orders of magnitude smaller than Förster rate γ_F. This gives us a reason to believe that for a wide range of hybrid carbon materials, the main mechanism of energy transfer from the dye molecule to graphene is the Förster mechanism. This is where we will focus our attention. We consider the process of excitation energy transfer from a dye molecule to a sheet of graphene. In the light field of an electromagnetic wave, a transient dipole moment in a dye molecule is generated. At the same time,

a transition charge density is generated in the graphene. The interaction (the Förster coupling) between the donor (dye molecule) and acceptor (graphene) can be seen as an of the molecular interaction between the transition dipole of the donor $\vec{d}_M^D = -e\int d\vec{r}_1 \psi_M^{l^*}(\vec{r}_1)\vec{r}_1\psi_M^h(\vec{r}_1)$ (where $\psi_M^{l^*}(\vec{r}_1)$ and $\psi_M^h(\vec{r}_1)$ the wave function for states dye molecule (donor)) and the transition charge density $\rho(\vec{r}_2) = -e\psi_{\vec{k}_i}^{v^*}(\vec{r}_2)\psi_{\vec{k}_f}^c(\vec{r}_2)$ (where $\psi_{\vec{k}_i}^{v^*}(\vec{r}_2)$ and $\psi_{\vec{k}_f}^c(\vec{r}_2)$ the wave function for states of the acceptor (graphene)). Therefore the matrix element for this interaction is given by the next expression

$$V = \vec{d}_M^D \cdot \nabla\Phi, \tag{4}$$

where Φ is the electrostatic potential at the point $\vec{r}$ (the position of the donor) due to the charge density $\rho(\vec{r}_2)$ and is given by

$$\Phi(\vec{r}) = \frac{1}{4\pi\varepsilon_0}\int d\vec{r}_2 \frac{\rho(\vec{r}_2)}{|\vec{r}-\vec{r}_2|}. \tag{5}$$

As a result of this energy transfer, an electron in valence band of graphene with wave vector $\vec{k}_i$ is excited to conduction band of graphene at the level with wave vector $\vec{k}_f = \vec{k}_i + \vec{q}$ (where $\hbar\vec{q}$ is the momentum transferred to graphene). The rate of this energy transfer γ_F can be calculated using the Fermi golden rule and given by the next expression

$$\gamma(\Delta E_M) = \frac{2\pi}{\hbar}\sum_{\vec{k}_i}\sum_{\vec{q}}\left|V_{\vec{k}_i\vec{q}}\right|^2 \delta\left(E_{\vec{k}_i+\vec{q}}^+ - E_{\vec{k}_i}^- - \Delta E_M\right), \tag{6}$$

where $V_{\vec{k}_i\vec{q}}$ is the matrix element of the transition of a graphene electron from an energy level with a wave vector $\vec{k}_i$ to the a level with a wave vector $\vec{k}_i + \vec{q} = \vec{k}_f$, ΔE is the emission energy of the dye molecule (the HOMO-LUMO gap, Fig. 2) to graphene.

The energies an electron in conduction (+) and valence (-) bands of graphene are given by [20]

$$E_{\vec{k}}^{\pm} = \pm\gamma_0\sqrt{1+4\cos\left(k_y a/2\right)\cos\left(k_x\sqrt{3}a/2\right)+4\cos^2\left(k_y a/2\right)}, \tag{7}$$

where γ_0 is the hopping integral for graphene, $a = l_{C-C}\sqrt{3}$ (l_{C-C} = 1.42A^0 is the C-C bond length of graphene, a = 0.246 nm) [20, 21]. So, denoting the deviation of electron wave vector from a *K*-point as $\vec{k}$ and carrying out an expression around the *K*-point, we get from (7)

$$E_{\vec{k}}^{\pm} = \pm\frac{\sqrt{3}}{2}k\gamma_0 = \pm\hbar v_F k, \tag{8}$$

where $k = \sqrt{k_x^2 + k_y^2}$, v_F is a Fermi velocity.

The crystal lattice of graphene is a combination of two interpenetrating lattices of Brave A and B with an elementary cell in the form of a regular rhombus (Figs. 3, 4). The period of these lattices is equal to $l_{C-C}\sqrt{3}$.

The wave function of the $\vec{k}$ – *th* orbital of graphene is given by a linear combination of two Bloch waves built on these sublattices [17–19]

$$\Psi_{\vec{k}}^{\pm}(\vec{r}) = \frac{1}{\sqrt{2N}}\left[\sum_{\vec{R}_A} e^{i\vec{k}\cdot\vec{R}_A}\chi_A\left(\vec{r}-\vec{R}_A\right)\mp\right.$$

$$\left.\mp e^{i\delta_{\vec{k}}}\sum_{\vec{R}_B} e^{i\vec{k}\cdot\vec{R}_B}\chi_B\left(\vec{r}-\vec{R}_B\right)\right], \tag{9}$$

where the (+) sign in $\Psi_{\vec{k}}^{\pm}(\vec{r})$ holds the conduction band (π* band) and the (–) sign holds for the valence band (π band). The phase factor $\delta_{\vec{k}}$ is defined by the relation $\delta_{\vec{k}} = \tan^{-1}\left(k_x/k_y\right) = \varphi_{\vec{k}}$ ($\varphi_{\vec{k}}$ is the angle that vector $\vec{k}$ makes with the *x*–axis) [21].

Using this wave function of graphene (9) the following expression for the matrix element $V_{\vec{k}_i\vec{q}}$ can be obtained [17-19]

$$\left|V_{\vec{k}_i\vec{q}}\right|^2 = \frac{e}{8\varepsilon_0^2 a^2}\left[1-\cos\left(\varphi_{\vec{k}_i+\vec{q}} - \varphi_{\vec{k}_i}\right)\right]\left|\vec{d}_M^D\left(i\hat{\vec{q}}+\hat{\vec{k}}\right)\right|^2 e^{-2qR}, \tag{10}$$

where $\varphi_{\vec{k}_i}$ and $\varphi_{\vec{k}_i+\vec{q}}$ are polar angles of the two-dimensional wave vector $\vec{k}_i$ and $\vec{k}_i+\vec{q}$, respectively; where *R* is the distance between dye molecule and graphene plane.

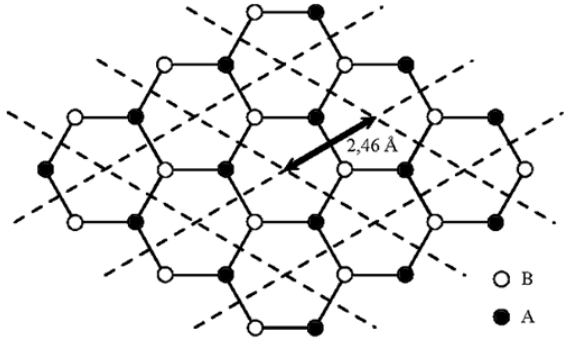

Fig. 3. The unit cell of graphene and the vector of translation of Brave lattices A and B [20]

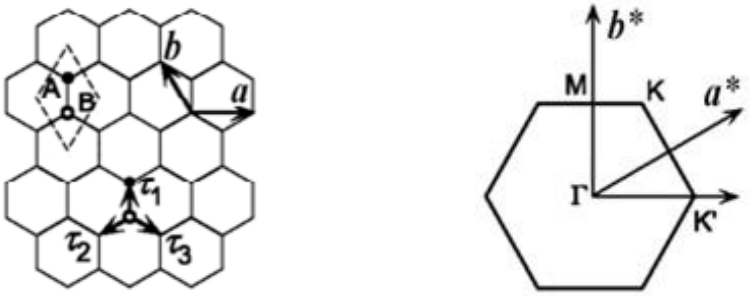

Fig. 4. Graphene lattice and its first Brillouin zone [20]

By substituting (10) into (6), we can obtain the following expression for the rate of energy transfer from the dye molecule (fluorophore) to graphene

$$\gamma_F\left(R,\Delta E_M\right)=\frac{\pi e^2}{4\hbar\varepsilon_0^2 a^2}\sum_{\vec{k}_i}\sum_{\vec{q}}\left|\vec{d}_M^{\,D}\cdot\left(i\hat{\vec{q}}+\hat{\vec{k}}\right)\right|^2 e^{-2qR}\left[1-\cos\left(\varphi_{\vec{k}_i+\vec{q}}-\varphi_{\vec{k}_i}\right)\right]\delta\left(E^+_{\vec{k}_i+\vec{q}}-E^-_{\vec{q}}-\Delta E_M\right). \qquad (11)$$

The sum over $\vec{k}_i$ in the equation (11) can be converted into an integral

$$\sum_{\vec{k}_i}\left[1-\cos\left(\varphi_{\vec{k}_i+\vec{q}}-\varphi_{\vec{k}_i}\right)\right]\delta\left(E^+_{\vec{k}_i+\vec{q}}-E^-_{\vec{q}}-\Delta E_M\right)=$$

$$=\frac{a}{4\pi^2}\int d\vec{k}_i\left[1-\frac{\vec{k}_i\left(\vec{k}+\vec{q}\right)}{\left|\vec{k}\right|\left|\vec{k}+\vec{q}\right|}\right]\delta\left(E^+_{\vec{k}_i+\vec{q}}-E^-_{\vec{q}}-\Delta E_M\right)=F\left(\vec{q}\right) \qquad (12)$$

and expression (11) can be written at the form

$$\gamma_F\left(R,\Delta E_M\right)=\frac{\pi e^2}{4\hbar\varepsilon_0^2 a^2}\sum_{\vec{q}}\left|\vec{d}_M^{\,D}\cdot\left(i\hat{\vec{q}}+\hat{\vec{k}}\right)\right|^2 e^{-2qR}F\left(\vec{q}\right). \qquad (13)$$

Moving to the new variable $\vec{k}_i'=\vec{k}_i+\vec{q}/2$ and using equation (8), we obtain the following expression for $F\left(\vec{q}\right)$ [17–19]

$$F\left(\vec{q}\right)=\frac{a}{4\pi^2\hbar v_F}\int d\vec{k}'\left[1-\frac{\left(\vec{k}'-\frac{\vec{q}}{2}\right)\left(\vec{k}'+\frac{\vec{q}}{2}\right)}{\left|\vec{k}'-\frac{\vec{q}}{2}\right|\left|\vec{k}'+\frac{\vec{q}}{2}\right|}\right]\delta\left(\left|\vec{k}'-\frac{\vec{q}}{2}\right|+\left|\vec{k}'+\frac{\vec{q}}{2}\right|-\frac{\Delta E_M}{\hbar v_F}\right). \tag{14}$$

Chosing the direction of $\vec{q}$ as the *x*-axis and then make another charge of variable to $\vec{r}$ given by $\vec{r}=2\vec{k}'/q$ we get

$$F\left(\vec{q}\right)=\frac{aq^2}{16\pi^2\hbar v_F}\int d\vec{r}\left[1-\frac{\left(\vec{r}-\hat{\vec{i}}\right)\left(\vec{r}+\hat{\vec{i}}\right)}{\left|\vec{r}-\hat{\vec{i}}\right|\left|\vec{r}+\hat{\vec{i}}\right|}\right]\delta\left[\left(\frac{q}{2}\left|\vec{r}+\hat{\vec{i}}\right|+\left|\vec{r}-\hat{\vec{i}}\right|\right)-\frac{\Delta E_M}{\hbar v_F}\right], \tag{15}$$

this may be rewritten at the form

$$F\left(\vec{q}\right)=\frac{aq^2}{8\pi^2\hbar v_F}\int_{-\infty}^{\infty}dx\int_0^{\infty}dy\left[1-\frac{x^2+y^2-1}{\sqrt{\left(x-1\right)^2+y^2}\sqrt{\left(x+1\right)^2+y^2}}\right]\delta\left[\frac{q}{2}\left(\sqrt{\left(x-1\right)^2+y^2}+\sqrt{\left(x+1\right)^2+y^2}\right)-\frac{\Delta E_M}{\hbar v_F}\right]. \tag{16}$$

Going from eq.(16) to elliptical coordinates using the relation $x=\mu\nu,\quad y=\sqrt{\left(\mu^2-1\right)\left(1-\nu^2\right)}$, we will rewrite (16) in the form

$$F\left(\vec{q}\right)=\frac{aq^2}{4\pi\hbar v_F}\int_1^{\infty}d\mu\int_{-1}^{1}d\nu\sqrt{\frac{1-\nu^2}{\mu^2-1}}\delta\left(q\mu-\frac{\Delta E_M}{\hbar v_F}\right). \tag{17}$$

After calculating the integrals in (17) we get the following relation for $F\left(\vec{q}\right)$ [19]

$$F\left(\vec{q}\right)=\frac{aq^2\Theta\left(\Delta E_M-q\hbar v_F\right)}{8\pi\sqrt{\Delta E_M^2-\left(q\hbar v_F\right)^2}}. \tag{18}$$

Substitution the above result (18) into equation (13), replace the sum over $\vec{q}$ by an integral, and use $\vec{d}_M^{\,D}=d_x\hat{\vec{i}}+d_y\hat{\vec{j}}+d_z\hat{\vec{k}}$, we get the following expression for the Förster rate of energy transfer γ_F from dye molecule to graphene [19]:

$$\gamma_F\left(R,\Delta E_M\right)=\frac{e^2\left(d_x^2+d_y^2+d_z^2\right)}{128\pi\hbar\varepsilon_0^2}\int_0^{\Delta E_M/\hbar v_F}dq\frac{e^{-2qR}q^3}{\sqrt{\Delta E_M^2-\hbar^2q^2v_F^2}}. \tag{19}$$

Eq. (19) can be used to calculate the Forster energy transfer rate in the next systems: dye molecule-graphene, functionalized graphene, and other systems.

Although, as shown in [16], for a wide range of hybrid carbon materials, for example porphyrin-functionalized graphene and perylene-functionalized graphene, the Dexter rate is expected to be approximately 4 orders of magnitude smaller than the Förster rate. For some materials, it is possible that the Dexter

energy transfer mechanism may play an important role in the energy transfer process and therefore should also be considered. Therefore, we briefly dwell on the description on this mechanism of energy transfer. Dexter energy transfer, as we moted earlier, is a mechanism which an excited electron is transferred from dye molecule (donor) to a second molecule (acceptor) via a non-radiative path. This process requires a wavefunction overlap between the donor and acceptor. This mechanism take place only occur at short distances between donor and acceptor, typically within 10 Å [15, 22]. Dexter applied the time-dependent perturbation theory of quantum mechanics to calculate the transition probability (energy transfer rate constant), and obtained a formula for γ_D that can be written as follows (using Fermi's golden rule) [15]

$$\gamma_D = \frac{2\pi}{\hbar}\left|\left\langle H_{if}\right\rangle\right|^2 \rho(E), \tag{20}$$

where $\left\langle \hat{H}_{if} \right\rangle$ is the matrix element of the perturbation of Hamiltonians between the initial (*i*) and final (*f*) states of system, $\rho(E)$ is the density of states. If the initial state (*i*) is described a wave function Ψ_i and final state (*f*) – Ψ_f the equation (20) may be described the next form

$$\gamma_D = \frac{2\pi}{\hbar}\rho(E)\left|\int \Psi_i^* \hat{H} \Psi_f d\tau\right|^2. \tag{21}$$

Hamiltonian $\hat{H}$ may be written at the form (coulomb potential energy of two charges)

$$\hat{H} = \frac{e^2}{4\pi\varepsilon\varepsilon_0 r_{12}}. \tag{22}$$

The wave function of electrons may be presentation at the form

$$\Psi = \Psi(r,\sigma) = \varphi(\vec{r})\chi(\sigma), \tag{23}$$

where $\varphi(\vec{r})$ $\left(\varphi \propto \exp(-R)\right)$ is radial and $\chi(\sigma)$ is the spin part of the electron wave function (23), respectively. Ignoring the spin orientation we consider electrostatic interaction between of two charges clouds $Q'(\vec{r}_1) = \varphi_D'^*(\vec{r}_1)\varphi_A'(\vec{r}_1)$ and $Q(\vec{r}_2) = \varphi_D^*(\vec{r}_2)\varphi_A(\vec{r}_2)$ and can write the Dexter transition probability (the rate of Dexter energy transfer) in the next form [15]

$$\gamma_D = \frac{2\pi}{\hbar} Z^2 \int f_D(E) F_A(E) dE, \tag{24}$$

where $\int f_D(E)\, f_A(E) dE$ is spectroscopic overlap integrals, measure of the donor-emission and accepter absorption ($f_D(E)$ the donor emission spectrum, and $f_A(E)$ the acceptor absorption emission spectrum); Z^2 has the dimensions of energy squared and may be written at the form [15]:

$$Z^2 = \frac{e^4}{\left(4\pi\varepsilon\varepsilon_0\right)^2}\sum_i\sum_f\left|\int Q'(\vec{r}_1)\frac{1}{\vec{r}_{12}}Q'(\vec{r}_2)\,d\tau_{12}\right|^2_{if}. \tag{25}$$

After calculation integral in eq. (25), Dexter received the next form for the parameter Z^2 [15]:

$$Z^2 = \frac{Ye^4}{\left(4\pi\varepsilon\varepsilon_0\right)^2 R_0^2}\exp\left\{-\frac{2R}{L}\right\}, \tag{26}$$

where Y is a dimensionless quantity <<1 which takes account of the cancellation as a result of sign changes in wave functions; L is an "effective average Bohr radius" for the excited and unexcited states of the donor (*D*) and acceptor (*A*) molecules; R_0 is "a critical transfer distance" in the sense that, for an isolated donor-acceptor pair separated by R_0, the energy transfer occurs with the same rate as spontaneous deactivation in the donor.

Thus, the final expression for the Dexter energy transfer rate can be written as [15, 22, 25]:

$$\gamma_D = \frac{Ye^4\int f_D(E)\, f_A(E) dE}{\left(4\pi\varepsilon\varepsilon_0\right)^2 R_0^2}\exp\left\{-\frac{2R}{L}\right\}. \tag{27}$$

So, the Dexter energy transfer rate γ_D with an increase in the distance between the donor and the acceptor *R*, it decreases exponentially

$$\gamma_D \propto \exp\left\{-\frac{2R}{L}\right\}. \quad (28)$$

RESULTS OF CALCULATIONS AND DISCUSSION

In this section, we will consider the original results of our research. Now let's apply the theoretical results obtained above for the analysis of energy transport in specific systems. As an example, let's choose a system of graphene - a dye molecule. We will proceed from the obtained eq. (19). Provided that $\mu_x = \mu_M \cos\alpha \sin\beta, \mu_y = \mu_M \sin\alpha \sin\beta, \mu_z = \mu_M \cos\beta$ (Fig. 5) we will average $\gamma_F\left(R, \Delta E_M\right)$ over all possible orientation of donor transition dipole moment, we get

$$\left\langle \gamma_F\left(R, \Delta E_M\right)\right\rangle \equiv \left\langle \gamma_F \right\rangle = \\ = \frac{e^2\mu_M^2}{96\pi\hbar\varepsilon_0^2} \int_0^{\Delta E_M/\hbar v_F} dq \frac{e^{-2qR} q^3}{\sqrt{\Delta E_M^2 - \hbar^2 q^2 v_F^2}}, \quad (29)$$

where μ_M is donor transition dipole moment averaged over possible orientations.

When $q \simeq 1/2R$ (for large values of $q \to 0$, we can neglected $\hbar^2 q^2 v_F^2 \simeq \frac{\hbar^2 v_F^2}{4R^2} \to 0$) comparison with ΔE_M^2 and evaluate the integral in eq. (29) by extending the upper limit of the integral to infinity ($\frac{\Delta E_M}{\hbar v_F} \to \infty$) to get

$$\left\langle \gamma_F \right\rangle = \frac{e^2\mu_M^2}{96\pi\hbar\varepsilon_0^2\Delta E_M} \int_0^\infty q^3 e^{-2qR} dq, \quad (30)$$

$$\int_0^\infty q^3 e^{-q2R} dq = \frac{3!}{(2R)^4} = \frac{6}{16R^4} = \frac{3}{8R^4}. \quad (31)$$

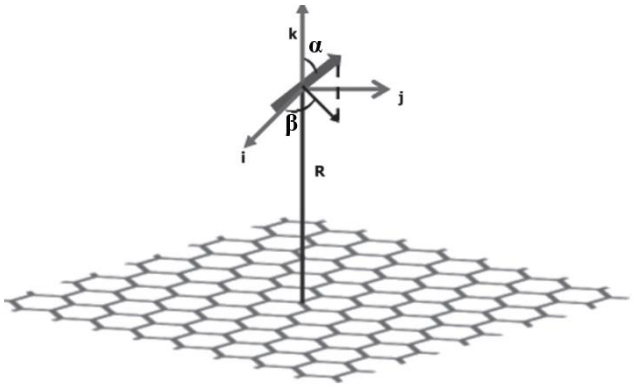

Fig. 5. Schematic of the donor (dye molecule)-acceptor (graphene) system showing the transition dipole of the dye molecule and the graphene lattice. In the figure the angles (α, β) the transition dipole moment vector makes on the coordinate axes

Substituting eq. (31) into eq. (30), we obtain the following analytical expression for the average energy transfer rate from dye molecule to graphene for large values of *R*

$$\left\langle \gamma_F \right\rangle = \frac{e^2\mu_M^2}{256\pi\Delta E_M\hbar\varepsilon_0^2 R^4} = \frac{1}{256\pi}\frac{\Delta E_M}{\hbar}\left(\frac{R_0}{R}\right)^4 \quad (32)$$

where $R_0 = \sqrt{\frac{e\mu_M}{\varepsilon_0\Delta E_M}}$.

Now we consider the eq. (30) in more detail. it can be rewritten in the following form If you enter in (30) replacement

$$q = \frac{\Delta E_M}{\hbar v_F} x, \quad dq = \frac{\Delta E_M}{\hbar v_F} dx \tag{33}$$

$$\left\langle \gamma_F \right\rangle = \frac{e^2 \mu_M^2}{96\pi\hbar\varepsilon_0^2 \Delta E_M} \left(\frac{\Delta E_M}{\hbar v_F} \right)^4 \int_0^1 \frac{x^3}{\sqrt{1-x^2}} \exp\left\{ -\frac{2\Delta E_M}{\hbar v_F} Rx \right\} dx. \tag{34}$$

If you enter the designation

$$\alpha_1 = \frac{e^2 \mu_g^2}{96\pi\hbar\varepsilon_0^2 \Delta E_M} \left(\frac{\Delta E_M}{\hbar v_F} \right)^4, \quad \alpha_2 = \frac{2\Delta E_M}{\hbar v_F}, \tag{35}$$

then eq. (34) can be written in the following form:

$$\left\langle \gamma_F \right\rangle = \alpha_1 \int_0^1 \frac{x^3 e^{-\alpha_2 Rx}}{\sqrt{1-x^2}} dx. \tag{36}$$

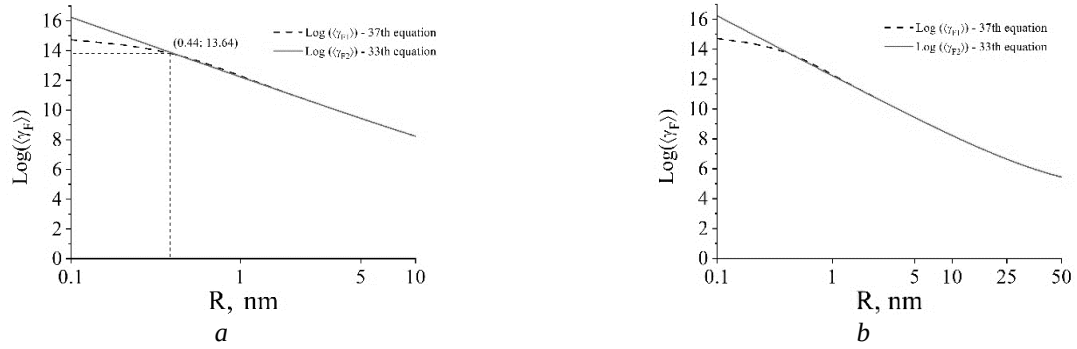

Fig. 6. Comparison between curves of average distance dependence rate of energy transfer $\left\langle \gamma_F \right\rangle$ in the system Pyrene–graphene, built for exact (36) and approximation eq. (32). *a* – for the small distance R; *b* – for long range approximation

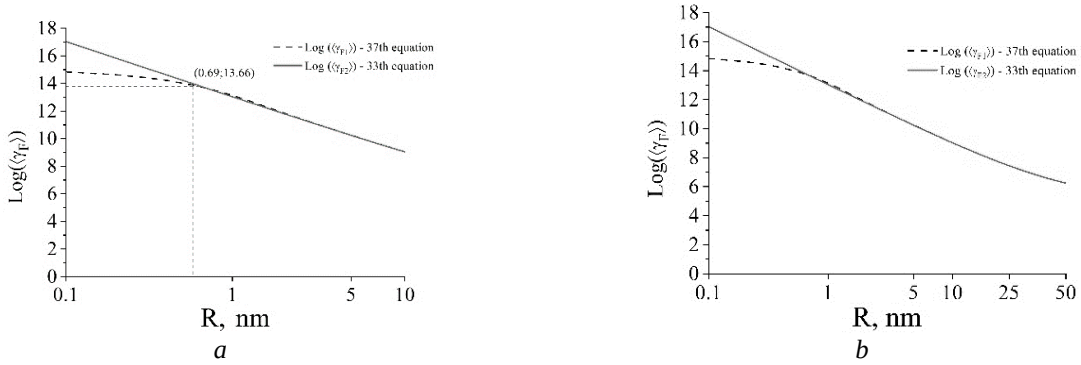

Fig. 7. Comparison between curves of average distance dependence rate of energy transfer $\left\langle \gamma_F \right\rangle$ in the system Nile blue – graphene, built for exact (36) and approximation eq. (32). *a* – for the small distance *R*; *b* – for long range approximation

Eq. (32) and eq. (36) can be used to calculate distance dependence of the rate of Förster energy transfer average over possible orientation on donor transition dipole moment of due molecule $\langle \gamma_F \rangle$. Let us emphasize that eq. (36) is exact, and eq. (32) is approximate.

As an illustration of the use of formulas (32) and (36), we calculate the average distance dependence rate of energy transfer in the system pyrene–graphene (Fig. 6) and Nile blue – graphene (Fig. 7). From the experimental emission spectra available for the dyes [24], one finds that the fluorescence maximum for pyrene occurs at $\Delta E_M = \hbar\Omega_{\max} = 3.2\,\text{eV}$ and Nile blue – $\Delta E_M = 2.0$ eV.

One can see from Fig. 6–7 for small distances ($R < 0.44$ nm (4.4 Å) for system pyrene –graphene; $R < 0.69$ nm (6.9 Å) for system Nile blue – graphene is a difference in the results given by the exact and approximate formulas. Therefore, in this range it is most likely necessary to use the exact formula (33), which we obtained for further calculations.

CONCLUSION

In this paper we analyzed inductive–resonance energy transfer in hybrid carbon nanostructures and calculate the distance dependence of the Förster energy transfer rate in the system dye molecule–graphene. Combining first-principle calculations characterizing the hybrid carbon nanomaterial with tight-binding-based consideration of graphene wave functions allows us to obtain an analytical expression for the Förster energy transfer rate. We constructed graphical dependences of the Förster energy transfer rate on the distance R between substrate (graphene) and dye molecule for several materials. Our calculations reveal strongly efficient Förster coupling with rates in the range of fs^{-1} (femtosecond^{-1}). In contrast, the Dexter energy transfer mechanism is found to be negligibly small due to small overlap between the involved strongly localized substrate and molecule orbital functions. The obtained results can be applied to other carbon-based hybrid nanostructures and in general to the description of energy transfer processes in molecular functionalized nanostructures, once the molecular dipole moment and the substrate-molecule separation are known. In this way, these considered pyrene-graphene systems, Nile blue – graphene system are often used as test systems for calculations, since many parameters of this system are known. For pyrene-graphene $R < 0.44$ nm and Nile blue-graphene $R < 0.69$ nm, we found a discrepancy in the calculation of energy transfer between approximate and exact equations. From our calculations, we can draw conclusions that when studying energy transfer over short distances, it is necessary to use the exact formula and not the approximation in R^{-4}. In the following studies, it is desirable to develop a theory for accurate calculations of energy transfer over short distances R^{-4}.

ACKNOWLEDGEMENT

The authors acknowledge Silvio Osella for insightful discussions and careful reading the manuscript.

Індуктивно-резонансний трансфер енергії в гібридних вуглецевих наноструктурах

О.Ю. Семчук, О.О. Гаврилюк, А.А. Білюк

Інститут хімії поверхні ім. О.О.Чуйка Нціональної академії наук України
вул. Генерала Наумова, 17, Київ, 03164, Україна, aleksandr1950@meta.ua

Спираючись на перші принципи, ми показали, що вирішальну роль у передачі енергії від молекули флюорофора до вуглецевої підкладки (графену) відіграє індуктивно-резонансний механізм передачі енергії (механізм Фьорстера). Швидкість передачі енергії по механізму Фьорстера можна розрахувати аналітично за допомогою золотого правила Фермі із залежними від імпульсу початковими та кінцевими станами графенових підкладок і станами HOMO (найвища зайнята молекулярна орбіталь) і LUMO (найменша

незайнята молекулярна орбіталь) молекули барвника. Поєднання розрахунків, що характеризують гібридні вуглецеві наноматеріали, з розглядом хвильових функцій графену на основі міцного зв'язку дозволило нам отримати аналітичний вираз для швидкості передачі енергії Фьорстера. Побудовано графічні залежності швидкості передачі енергії Фьорстера від відстані R між підкладкою (графеном) і молекулою барвника для кількох матеріалів. Отримані результати можуть бути застосовані для опису процесів передачі енергії в молекулярно-функціоналізованих наноструктурах, якщо відомі молекулярний дипольний момент і розділення субстрат-молекула.

***Ключові слова**: графен, вуглецеві нанотрубки, функціоналізований графен, молекула барвника, золоте правило Фермі, швидкість передачі енергії, молекули флуорофора, механізм Фьорстера, механізм Декстера, оптоелектроніка*

REFERENCES

1. Kenfack G.M.D., Nya F.T., Bouba M.O., Malloum A., Conradie J. Optoelectrical, electronic, and thermodynamic DFT study of a carbon nanoring and its derivative: application as active layer material in organic solar cell performance improvement and nonlinear optics. *J. Mol. Model.* 2022. **29**(1): 1.
2. Kubba R. *Application of quantum mechanical calculations and symmetry in chemistry; vibration frequencies, corrosion inhibition.* (B P International, 2021).
3. Reich S., Thomsen C., Maultzsch J. *Carbon nanotubes: basic concepts and physical properties*. (John Wiley & Sons: New Jersey, 2008).
4. Ghosh S.K., Chattaraj P.K. *Concepts and methods in modern theoretical chemistry: statistical mechanics*. (Florida: Taylor & Francis Group, 2019).
5. Malic E., Knorr A. *Graphene and carbon nanotubes: ultrafast optics and relaxation dynamics.* (Willey-VCH: Berlin, 2013).
6. Rai P., Shukla V.K. *Carbon material-based nanoscale optics and plasmonics.* (Singapore: Springer, 2024).
7. Malic E., Weber C., Richter M., Atalla V., Klamroth T., Saalfrank P., Reich S., Knorr A. Microscopic model of the optical absorption of carbon nanotubes functionalized with molecular spiropyran photoswitches. *Phys. Rev. Lett.* 2011, **106**: 097401.
8. Nakagawa Y., Yu B., Niidome Y., Hayashi K., Staykov A., Yamada M., Nakashima T., Kawai T., Fujigaya T., Shiraki T. Photoisomerization of covalently attached diarylethene on locally functionalized single-walled carbon nanotubes for photoinduced wavelength switching of near-infrared photoluminescence. *J. Phys. Chem. C.* 2022. **126**(25): 10478.
9. Yang M., Ye Z., Sun C. -H., Zhu L., Hajizadegan M., Chen P. -Y. A lightweight, zero-power intermodulation sensor based on the graphene oscillator. *IEEE Sens. J.* 2023. **23**(3) 3243.
10. Koyama T., Sugiura J., Koishi T., Ohashi R., Asaka K., Saito, T., Gao Y., Okada S., Kishida H. Excitation energy transfer by electron exchange via two-step electron transfer between a single-walled carbon nanotube and encapsulated magnesium porphyrin. *J. Phys. Chem. C.* 2020. **124**(35): 19406.
11. Roquelet C., Garrot D., Lauret J.S., Voisin C., Alain-Rizzo V., Roussignol P., Delaire J.A., Deleporte E. Quantum efficiency of energy transfer in noncovalent carbon nanotube/porphyrin compounds. *Appl. Phys. Lett.* 2010. **9**: 141918.
12. Ernst F., Heek T., Setaro A., Haag R., Reich S. Energy transfer in nanotube–perylene complexes. *Adv. Funct. Mater.* 2012. **22**(18): 3921.
13. Gaudreau L., Tielrooij K.J., Prawiroatmodjo G.E., Osmond J., de Abajo F.J.G., Koppens F.H. Universal distance-scaling of nonradiative energy transfer to graphene. *Nano Lett.* 2013. **13**(5): 2030.
14. Forster T. Zwischenmolekulare energiewanderung und fluoreszenz. *Ann. Phys.* 1948. **437**(1–2): 55.
15. Dexter D.L. A Theory of sensitized luminescence in solids. *J. Chem. Phys.* 1953. **21**(5): 836.
16. Malic E, Appel H., Hoffman O.T., Rubio A. Forster-induced energy transfer in functionalized graphene. *J. Chem. Phys.* 2014. **118**(17): 9283.
17. Swathi R.S., Sebastian K.L. Distance dependence of fluorescence energy transfer. *J. Chem. Sci.* 2009. **121**: 777.
18. Swathi R.S., Sebastian K.L. Excitation energy transfer from dye molecule to doped graphene. *J. Chem. Sci.* 2012. **124**: 233.
19. Swathi R.S., Sebastian K.L. Resonance energy transfer from a dye molecule to graphene has (distance)$^{-4}$ dependence. *J. Chem. Phys.* 2009. **139**: 086101.

20. Rathinavel S., Priyadharshini K., Panda D. A review on carbon nanotube: An overview of synthesis, properties, functionalization, characterization, and the application. *Mater. Sci. Eng. B.* 2021. **268**: 115095.
21. Ali M.A. *Quantum Hall Effect on Dirac electrons in modulated graphene*. (arXiv, 2023).
22. Murphy C.B., Zhang Y., Troxler T., Ferry V., Martin J.J., Jones (Jr) W.E. Probing Forster and Dexter energy–transfer mechanisms in fluorescent conjugated polymer chemosensors. *J. Phys. Chem B.* 2004. **108**(5): 1537.
23. Gradshteyn I.S., Ryzhik I.M. *Table of integrals, series, and products.* (Elsevier, 2014).
24. Orucu H., Acar N. Effects of substituent groups and solvent media on Pyrene in ground and excited states: A DFT and TDDFT study. *Comput. Theor. Chem*. 2015. **1056**: 11.
25. Skorjanc T., Shetty D., Valant M. Covalent Organic polymers and frameworks for fluorescence-based sensors. *ACS Sensors.* 2021. **6**(4): 1461.
26. Ma Y., Zhi L. Functionalized graphene materials: definitions, classification, and reparation strategies. *Acta Phys. -Chim. Sin.* 2022. **38**(1): 2101004.

Received 15.01.2024, accepted 03.09.2024